Results in Physics 16 (2020) 102822

Contents lists available at ScienceDirect

Results in Physics

journal homepage: www.elsevier.com/locate/rinp

All-optical wavelength division multiplexing amplifier based on vacuum induced nonreciprocal bistability in six-wave mixing process with a ring cavity

Kangkang Li, Yin Cai, Wei Li, Huanrong Fan, Shaohuan Ning, Siqiang Zhang, Yanpeng Zhang*

Key Laboratory for Physical Electronics and Devices of the Ministry of Education & Shaanxi Key Lab of Information Photonic Technique, Xi'an Jiaotong University, Xi'an 710049, China

ARTICLE INFO

Keywords:
Bistability
Nonlinear optics
Cavity feedback dressing effect
All-optical device

ABSTRACT

In this article, we experimentally investigate the nonreciprocal bistability (NB) of two six-wave mixing (SWM) processes inside of a ring cavity with a five-level rubidium atomic cell. The degree of NB can be analyzed by the nonreciprocal area (or non-overlapping area) including the frequency offset (in the x-direction) and the intensity difference (in the y-direction) between output states. The frequency offset between the two states of signals is resulting from the Kerr nonlinearity, while the cavity feedback dressing effect determines the intensity difference. Besides, the signals are amplified by the SWM polariton and vacuum induced enhancement. Based on the effect of NB, we study the realization of an all-optical wavelength division multiplexing amplifier (WDMA). The optical contrast and channel equalization radio of this WMDA is contributed from the degree of nonreciprocal area of output states of signals. Such results may have potential applications in all-optical devices and optical communication.

Introduction

Widely studied in applications, all-optical switching devices play an indispensable role in all-optical information processing [1–3]. Cavity quantum electrodynamics has attracted intensive attention in the last decades [4] because of the important applications in quantum optics and nonlinear optics. The phenomenon of vacuum induced transparency has been reported which can modify the transmission of an atomic ensemble with about 10 control photons [5]. A composite atom-cavity system can be configured by placing atoms inside an optical cavity to amplify the efficiency of nonlinear optical processes such as the intracavity dark-state polariton [6] and enhanced Kerr nonlinearity [7]. In recent years, many optical phenomena based on atomic coherence and quantum interference have attracted intensive attention. Compared with crystal, by photon-atom interfaces that matching to an atomic transition naturally, the generated photons with narrow-band and strong nonlinear optics response are more suitable for optical information processing [8]. Based on the multi-level atomic systems, multi-wave mixing (MWM) processes have been experimentally reported in all alkali atoms and various experimental schemes [8–16]. Besides, MWM processes have been reported along with the coexisting cavity modes of parametrically amplified MWM signals, in which a strong coupling beam renders a resonant and opaque medium nearly transparency while enhancing the nonlinearity [17,18]. With the combination of the electromagnetically induced transparency (EIT) effect and the optical cavity, many interesting effects, among which optical nonreciprocal bistability (NB) has been extensively studied, where cavity can provide feedback as an essential factor for the generation of NB [19,20]. Besides, NB also has observed experimentally in three or four levels of atomic systems inside an optical cavity [21–23], and a flip-flop converter is realized by using NB [23]. Moreover, in atomic vapor without a cavity using degenerate MWM, the optical phenomena of NB were reported [24–26] and used to realize a two-channel router [27]. In addition, the nonreciprocity of transmitted light was investigated in a moving photonic crystal via Faraday or nonlinear effects [28]. The influence of dark and bright states of vacuum Rabi splitting and nonreciprocity of the MWM process in a collective three- or four-level atomic-cavity coupling system have been reported [20,22]. Compare with the traditional NB [29,30] by scanning the input intensity of the cavity, a new kind of NB which is demonstrated through a two-dimension non-overlapping region on the transmitted spectrum versus the detuning of cavity or driving fields is proved to be more sensitive [31].

In this paper, we study the realization of an all-optical wavelength

* Corresponding author.
E-mail address: ypzhang@mail.xjtu.edu.cn (Y. Zhang).

https://doi.org/10.1016/j.rinp.2019.102822
Received 2 October 2019; Received in revised form 17 November 2019; Accepted 17 November 2019
Available online 22 November 2019

division multiplexing amplifier (WDMA) using the optical NB phenomena of vacuum induced enhancement six-wave mixing (SWM) process in a composite cavity-atom system. Different from the transport properties of photons in the conventional optical bistable system [19], all incident laser fields in our system need to satisfy the phase-matching conditions of SWM. Compared with NB phenomena in atomic vapor without a cavity, the vacuum Rabi splitting from cavity can effectively affect NB phenomena. Also, based on four-wave mixing, the SWM process can be manipulated by multi-dressing parametric and therefore have stronger nonlinear optic response. We theoretically and experimentally investigate the effect of NB by analyzing the non-overlapping area [22,23] of output states. By calculating the movement of the signal resonant peaks under different conditions, we found that the NB of SWM can be controlled by different parameters including detunings and powers of dressing beams. Besides, the competitive relationship between the NB and cavity, dressing enhancement (or suppression) of SWM is also observed significantly. Moreover, the two output states result from NB can be used to realize an all-optical WDMA.

Experimental details and basic theory

Experimental details

The experiment is implemented in a composite cavity-atom system where a thermal five-level ^{85}Rb atoms are confined in the optical ring cavity. Fig. 1(a) is a schematic diagram of the experimental setup in which the plate-concave mirrors M1, M2, and flat mirror M3 configure the ring cavity having a total length of 38 cm. The relevant energy levels are shown in Fig. 1(b). In this system, a probe laser beam $\boldsymbol{E}_1$ (frequency ω_1, wave vector $\boldsymbol{k}_1$, and Rabi frequency G_1) connects the lower transition $5S_{1/2}$ (F = 3, $|0\rangle$) to $5P_{3/2}$ ($|1\rangle$) with wavelength of 780 nm and vertically polarization. Two vertically polarized coupling fields $\boldsymbol{E}_2$ (ω_2, $\boldsymbol{k}_2$, and G_2) and $\boldsymbol{E}_4$ (ω_4, $\boldsymbol{k}_4$, and G_4) with wavelength of 776 nm, drive the upper transition $|1\rangle$ to $5D_{5/2}$ ($|2\rangle$) and $5D_{3/2}$ ($|4\rangle$), respectively. One vertically polarized coupling field $\boldsymbol{E}'_3$ (ω'_3, $\boldsymbol{k}'_3$, and G'_3) propagates along the optical axis of the cavity (indicated by the dashed line in Fig. 1(a)) and couple states $|1\rangle$ and $5S_{1/2}$ (F = 2, $|3\rangle$). Another vertically polarized coupling field $\boldsymbol{E}_3$ propagate in the opposite direction with $\boldsymbol{E}_1$, which has an angle of about 2° with $\boldsymbol{E}'_3$ beam and couple states $5S_{1/2}$ (F = 2, $|3\rangle$) and $|1\rangle$. Here, $\boldsymbol{E}_3$ and $\boldsymbol{E}'_3$ come from one laser source with a wavelength of 780 nm.

The plate-concave mirrors M_1, M_2, and flat mirror M_3 configure the ring cavity. The reflectivity of mirrors M_2 and M_3 are approximately 97.5% at 780 nm. A piezoelectric transducer (PZT) is mounted on the back of M_1 (with the reflectivity 99%) to adjust the cavity length. The 7 cm long rubidium vapor cell is placed in the middle of M_1 and M_2. The probe beam $\boldsymbol{E}_1$ with vertical polarization enters the cavity through polarized beam splitter and is reflected away by mirror RM. The temperature of the cell is set at 60 °C, corresponding to the atomic density of 2.498×10^{11} cm^{-3}. When the atomic cell is properly placed at the midpoint between M_1 and M_2, the five laser beams converge at the cell center where the diameters of the probe beam and pumping beams are about 0.3 mm and 0.5 mm, respectively. Only SWM signals with the specific propagation and horizontal polarization can circulate inside the ring cavity and can form cavity modes. The SWM signals are detected by one avalanche photodiode detector (APD) after transmitting out of the flat mirror M_3.

Since all the involved laser beams are linearly polarized, we just consider this five-level system, which is the simplest Zeeman sublevels [32,33]. There are two EIT windows in ladder-type subsystems $|0\rangle-|1\rangle-|2\rangle$ and $|0\rangle-|1\rangle-|4\rangle$. The frequency detunings of E_1, E_2 (E_4) and E_3 (E_3') are $\tilde{\Delta}_1$, $\tilde{\Delta}_2$ ($\tilde{\Delta}_4$) and $\tilde{\Delta}_3$ ($\tilde{\Delta}_3^{\text{prime}}$) ($\tilde{\Delta}_4 = \Omega_i - \omega_i$, i = 1, 2, 3, 4), Ω_i is the resonance frequency of the transition driven by E_i), respectively. Considering the thermal linewidth of the hot Rb vapor with velocity v (as shown in Fig. 1(a)) along the probe fields, the frequency of E_1, E_2, E_3, E'_3 and E_4 shift to ω_1-k_1v, $\omega_2 + k_2v$, $\omega_3 + k_3v$, $\omega'_3 + k'_3v$ and $\omega_4 + k_4v$, respectively when the Doppler effect is phenomenologically introduced to weak signals. As a result, the frequency detunings of E_1, E_2 (E_4) and E_3 (E'_3) shift to $\Delta_1 = \tilde{\Delta}_1 - k_1v$, $\Delta_2 = \tilde{\Delta}_2 - k_2v$ ($\Delta_4 = \tilde{\Delta}_4 - k_4v$) and $\Delta_3 = \tilde{\Delta}_3 + k_3v$ ($\Delta'_3 = \tilde{\Delta}'_3 + k'_3v$), respectively, where $\Delta_3 = \Delta'_3$. In the atomic vapor with all beams on, two phase-conjugate SWM signals (E_{S1} & E_{S2}) which satisfying the phase matching conditions $k_{S1} = k_1 + k_3 + k_3^{\text{prime}} + k_4 - k_4$ and $k_{S2} = k_1 + k_3 + k_3^{\text{prime}} + k_2 - k_2$, respectively. The SWM signals are generated at the center of the atomic cell and propagate along the optical axis of the cavity, which guarantees that they are mode-matched to the cavity and form the cavity modes.

Basic theory

Considering the Liouville pathway and using the scalar of the velocity v, the perturbation chains of E_{S1} and E_{S2} signals are shift to $\rho_{00}^{(0)} \xrightarrow{\omega_1} \rho_{10}^{(1)} \xrightarrow{-\omega'_3} \rho_{30}^{(2)} \xrightarrow{\omega_3} \rho_{10}^{(3)} \xrightarrow{\omega_4} \rho_{40}^{(4)} \xrightarrow{-\omega_4} \rho_{10}^{(5)}$ and $\rho_{00}^{(0)} \xrightarrow{\omega_1} \rho_{10}^{(1)} \xrightarrow{-\omega'_3} \rho_{30}^{(2)} \xrightarrow{\omega_3} \rho_{10}^{(3)} \xrightarrow{\omega_2} \rho_{20}^{(4)} \xrightarrow{-\omega_2} \rho_{10}^{(5)}$, respectively. By solving the density-matrix equations, the fifth-order density elements can be written as follows:

$$\rho_{10S1}^{(5)} = -(iG_1)(iG'_3)(iG_3)|G_4|^2/(d_1^3 d_3 d_4), \tag{1}$$

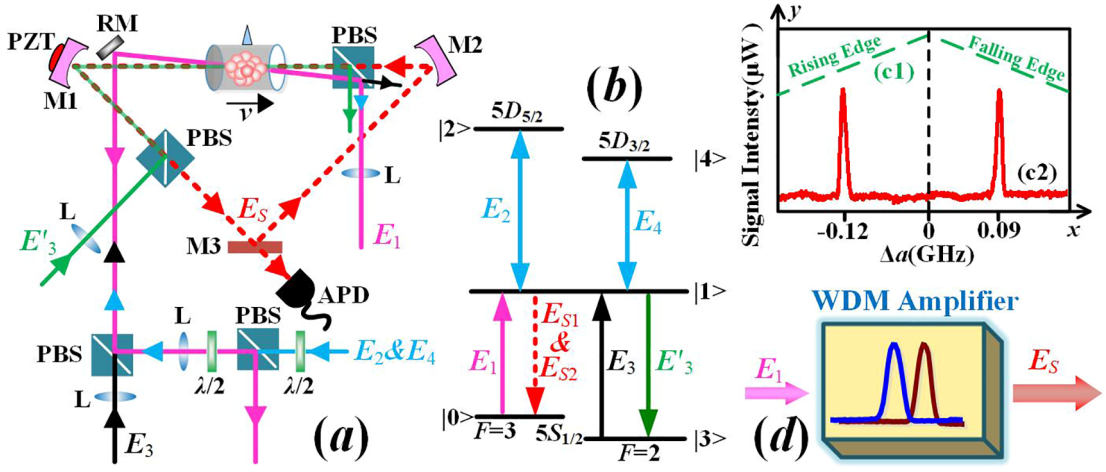

Fig. 1. (a) Experimental setup. PBS: polarizing beam splitters; F: optical lens; APD: avalanche photodiode detector; PZT: piezoelectric transducer; M1–M3: cavity mirrors; RM: high reflectivity mirror; l/2: half-wave plate. (b) Five–level energy system diagram for the laser coupling configuration in 85Rb vapor. (c1) Two arm ramps of one round trip. (c2) SWM signals by scanning Δ_4. (d) Schematic diagram of the all-optical wavelength division multiplexing amplifier.

$$\rho_{10S2}^{(5)} = -(iG_1)(iG_3')(iG_3)|G_2|^2/(d_1^3 d_3 d_2), \quad (2)$$

where $d_1 = \Gamma_{10} + i\Delta_1$, $d_2 = \Gamma_{20} + i(\Delta_1 + \Delta_2)$, $d_3 = \Gamma_{30} + i(\Delta_1\text{-}\Delta_3)$ and $d_4 = \Gamma_{40} + i(\Delta_1 + \Delta_4)$. Γ_{ij} is the transverse relaxation rate between states $|i\rangle$ and $|j\rangle$.

Since the generated SWM signals can circulate in the ring cavity, which forms the cavity modes, we analyze the NB behavior of SWM based on the cavity modes of SWM signals. Using the zero-order mode, the cavity modes can be dressed by both internal-dressing field E_1 and external-dressing fields E_2 and E_4. Besides, similar to the vacuum induced transparency reported in Ref. [17], the vacuum induced cavity dressing effect of atom-cavity coupling $gN^{1/2}$ (g is the single-atom–-cavity coupling strength and N is the atom number) is caused by the resonant fluorescence of E_1, which also can result in the cavity modes. G_{S1} and G_{S2} are the intensities of cavity feedback dressing (self-dressing), the cavity modes of E_{S1} and E_{S2} are given as

$$a_{S1} = -g\sqrt{N}\rho_{10S1}^{(5)}T/\left[\begin{array}{c} d_5(d_1 + g^2N/d_5 + |G_2|^2/d_2 \\ + |G_4|^2/d_4 + |G_{S1}|^2/\Gamma_{00}) \end{array}\right], \quad (3)$$

$$a_{S2} = -g\sqrt{N}\rho_{10S2}^{(5)}T/\left[\begin{array}{c} d_5(d_1 + g^2N/d_5 + |G_2|^2/d_2 \\ + |G_4|^2/d_4 + |G_{S2}|^2/\Gamma_{00}) \end{array}\right], \quad (4)$$

where $d_5 = \gamma + i(\Delta_1 - \Delta_{ac})$, γ is the decay rate for the cavity and $\Delta_{ac} = \Omega_1 - \omega_c$ is the frequency detuning with ω_c being the resonant frequency of the cavity, Γ_{00} represent the atomic population at the group state. T is the transmission coefficient of the output mirror M_3. The SWM cavity mode E_{S1} is generated in the electromagnetically induced absorption (EIA) window $\Delta_1 + \Delta_2 = 0$. Besides, with SWM polariton, the cavity mode of E_{S2} (Eq. (3)) is generated with EIA window $\Delta_1 + \Delta_4 = 0$ and circulates inside the cavity. The curves in Fig. 1(c2) is SWM cavity mode signal E_{S2} by scanning Δ_4 from negative to positive value, where the baseline is the mixing cavity modes of E_F (generation from four-wave mixing process with the phase-matching condition of $\boldsymbol{k}_F = \boldsymbol{k}_1 + \boldsymbol{k}_3 - \boldsymbol{k}'_3$) and E_{S1}. The peaks in Fig. 1(c2) are the cavity modes of E_{S2} which includes three parts: the SWM polariton due to the term $gN^{1/2}/d_5$, the enhancement of E_{S2} caused by cavity dressing term g^2N/d_5 and the external-dressing effect of E_4 in Eq. (4). The competition between the SWM polariton ($gN^{1/2}/d_5$) and the vacuum induced enhancement effect (g^2N/d_5) by the atom-cavity coupling strength ($gN^{1/2}$) can enhance the signals. The window $\Delta_1 - \Delta_{ac} = 0$ is labeled as a cavity transmission window, which comes from the internal-dressing term g^2N/d_5 of Eq. (3). In Fig. 1(c2), the left and right peaks belong to the signals of rising and falling edge in one frequency scanning round trip, respectively. The two-arm ramps of one round trip are shown in Fig. 1(c1) by scanning Δ_4 from 200 MHz to −200 MHz and then to 200 MHz again with $\Delta_2 = \Delta_{ac} = 0$. In Fig. 1(c), resulting from the different cavity feedback effect on two signal edges, the frequency offset between the central frequency of these two peaks is about 40 MHz. Therefore, these two different output states can be viewed as optical nonreciprocal bistability (NB). When folding the signals on the two edges from the maxima of the ramp curves in one round trip, two different output states exist a non-overlapping region (nonreciprocity area). This nonreciprocity area (S) includes two kinds of nonreciprocity: the frequency offset (in the x-direction) and the intensity difference (in y-direction), and can be divided into two parts: S_1 and S_2. We define the line width of the left and right signal peaks as Δ_L and Δ_R, respectively. When we treat the signal peaks as triangles, the nonreciprocity areas under the special conditions where the two signals not overlapped are calculated as

$$S = S_1 + S_2 \propto \Delta_L I_{up}/2 + \Delta_R I_{down}/2, \quad (5)$$

where $\Delta\upsilon = (\Delta_L + \Delta_R)/2$; I_{up} is the intensity of the signals from the rising edge of the ramp; I_{down} is the intensity of the signals from the falling edge.

The nonreciprocity of frequency offset in the x-direction is resulting from the cavity feedback dressing effect of SWM signals. The changing of the nonlinear refractive index $\Delta n'$ is given as follow

$$\Delta n' = N(n_{2up}I_{up} - n_{2down}I_{down}) = \Delta\sigma c/\omega_p l, \quad (6)$$

where $\Delta\sigma = \Delta\upsilon n_1 l/c$ is the phase delay, n_1 is the linear refractive index of the Rb cell, $l = 7$ cm is the length of the ^{85}Rb cell and $\Delta\upsilon$ is the frequency offset which can reflect the NB of the signals directly. n_{2up} and n_{2down} are the nonlinear refractive index of the cell related to the density of the ^{85}Rb vapor N. I_{up} and I_{down} represent the different feedback dressing intensities of signals on the rising and falling edges. Here, we consider $n_{2up} \approx n_{2down} \approx n_2$, where $n_2 = \mathrm{Re}\chi^{(3)}/(\varepsilon_0 c n_0)$ is the Kerr nonlinear coefficient with μ_{j0} is the nonlinear susceptibility, μ_{j0} is the dipole moment between $|j\rangle$ and $|0\rangle$ [34], ε_0 is dielectric constant and $\tilde{\rho}_{10}^{(3)}$ is the dressed density-matrix element. Therefore, the formula for $\Delta n'$ can be rewritten as

$$\Delta n' = Nn_2(I_{up} - I_{down}) = \Delta\sigma c/\omega_p l, \quad (7)$$

The changing of n_2 and the feedback dressing intensities of the I_{up} and I_{down}, are the function of the scanning fields and the changing dressing fields. By considering the self-Kerr effect and cross-Kerr effect, the dressed density-matrix elements $\tilde{\rho}_{10}^{(3)}$ is as follows

$$\tilde{\rho}_{10}^{(3)} = -iG_S|G_1|^2/\left[\Gamma_{00}\left(\begin{array}{c} d_1 + g^2N/d_5 + G_1^2/\Gamma_{00} \\ + G_2^2/d_2 + G_3^2/d_3 + G_4^2/d_4 \end{array}\right)^2\right], \quad (8)$$

By analyzing the above-mentioned equations, we can conclude that the self-Kerr effect is induced by G_S, whereas the cross-Kerr effect is induced by G_1. Besides, by considering the different cavity feedback dressing effects, the signals on the rising and falling edges will meet different enhancement (or suppression) conditions which can also advocate the effect of NB. Therefore, in y-direction, we investigate the intensity difference between the signal curves in the frequency-increasing and frequency-decreasing processes by the suppression and enhancement conditions of SWM. Firstly, the primary splitting is caused by external-dressing field $\boldsymbol{E}_2$. The corresponding eigenvalues are $\lambda_\pm = [\Delta_2 \pm (\Delta_2^2 + 4|G_2|^2)^{1/2}]/2$ and we can get the suppression and enhancement conditions as $\Delta_1 + \Delta_2 = 0$ and $\Delta_1 + \lambda_\pm = 0$, respectively. The second splitting is caused by the external-dressing field $\boldsymbol{E}_4$ whose corresponding eigenvalues are $\lambda_{+\pm} = [\Delta_4'^2 \pm (\Delta_4'^2 + 4|G_4|^2)^{1/2}]/2$ ($\Delta_4' = \Delta_4 - \lambda_+$), and the suppression and enhancement conditions are $\Delta_1 + \Delta_4' = 0$ and $\Delta_1 + \lambda_\pm + \lambda_{+\pm} = 0$, respectively. Thirdly, we consider the suppression and enhancement effect of cavity dressing by scanning the length of the cavity Δ_{ac} as $\Delta_1 + \Delta_{ac}' = 0$ ($\Delta_{ac}' = -\Delta_{ac} - \lambda_{+\pm}$) and $\Delta_1 + \lambda_\pm + \lambda_{+\pm} + \lambda_{++\pm} = 0$, where $\lambda_{++\pm} = [\Delta_{ac}'^2 \pm (\Delta_{ac}'^2 + 4|gN^{1/2}|^2)^{1/2}]/2$. Finally, we consider the splitting by the cavity feedback dressing effect of MWM. The suppression and enhancement conditions are $\Delta_1 + \Delta_1' = 0$ ($\Delta_1' = \Delta_S - \lambda_{++\pm}$, where Δ_S represents the detuning of SWM) and $\Delta_1 + \lambda_\pm + \lambda_{+\pm} + \lambda_{++\pm} + \lambda_{+++\pm} = 0$ ($\lambda_{+++\pm} = [(\Delta_1^{prime2} \pm \Delta_1^{prime2} + 4|G_S|^2)^{1/2}]/2$), respectively. The nonreciprocity of signal intensity resulting from the different cavity feedback dressing is influenced by the dressing effect of $\boldsymbol{E}_2$, $\boldsymbol{E}_4$ and cavity dressing by considering these suppression and enhancement conditions.

The central frequency offset means these two different states exist in two different central frequency position. Using these two different output frequency positions of signal and amplified action of the system, we can apply the proposed scheme as the all-optical wavelength division multiplexing amplifier as shown in Fig. 1(d). We, therefore, can use this WDMA to output two signal channels effectively.

Results

In our experiment results (Figs. 2–4), we observe the nonreciprocity area by folding signals along the central dashed line as shown in Fig. 1(c). Combining the experiment results, we mainly investigated the NB by analyzing the nonreciprocity area based on frequency offset $\Delta\upsilon$ and intensity difference ΔI, optical contrast and channel equalization

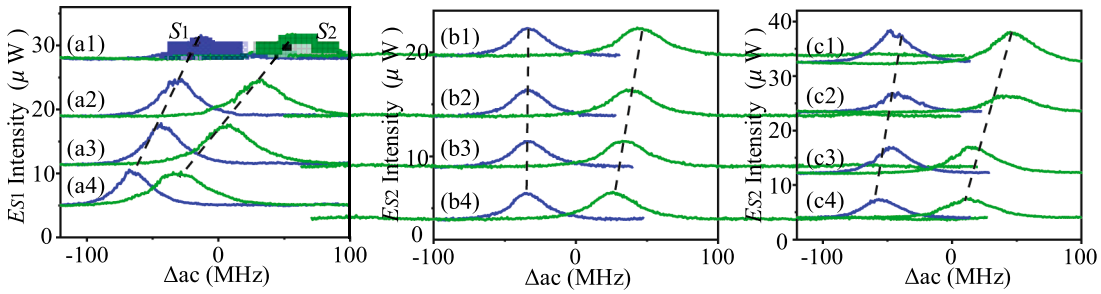

Fig. 2. Measured SWM signal versus Δac. (a1)–(a4) $\boldsymbol{E}_{S1}$ signals at discrete Δ_1 as 60 MHz, 30 MHz, 0 MHz, −30 MHz, respectively, with beam $\boldsymbol{E}_2$ blocked and $\boldsymbol{E}_4$ opened. (b1)–(b4) $\boldsymbol{E}_{S2}$ signals at discrete Δ_2 as 0 MHz, −30 MHz, −60 MHz, −90 MHz, respectively, with beam $\boldsymbol{E}_4$ blocked and $\boldsymbol{E}_2$ opened. (c1)–(c4) $\boldsymbol{E}_{S2}$ signals at discrete Δ_2 as 0 MHz, −30 MHz, −60 MHz, −90 MHz, respectively, with both $\boldsymbol{E}_4$ and $\boldsymbol{E}_2$ opened.

radio of two output states.

First, we investigate the NB of cavity modes of $\boldsymbol{E}_{S1}$ and $\boldsymbol{E}_{S2}$ by scanning cavity frequency Δ_{ac} under different experimental conditions and make a comparison among the cavity modes of $\boldsymbol{E}_{S1}$ and $\boldsymbol{E}_{S2}$. The signals in Fig. 2 are scanning Δ_{ac} from −100 MHz to 100 MHz and then to −100 MHz again by changing the voltage of the PZT on M_1 (ω_a). Fig. 2(a) is the cavity mode of $\boldsymbol{E}_{S1}$ at $\Delta_1 + \Delta_4 = 0$ when we open $\boldsymbol{E}_4$ and keep $\boldsymbol{E}_2$ blocked. The peaks represent the enhancement of cavity modes of $\boldsymbol{E}_{S1}$ caused by the cavity dressing (g^2N/d_5) and SWM polaritons ($gN^{1/2}/d_5$) in Eq. (3). As one can see, the two folded signals from one complete cycle are not completely overlapping, which have nonreciprocity areas of S_1 and S_2 in Fig. 2(a1). In Fig. 2(a1), the frequency offset $\Delta\nu$ in the x-direction is calculated as 71.7 MHz which is caused by the different feedback terms $|G_{S1}|^2/\Gamma_{00}$ at rising and falling edges in Eq. (3). The intensity value in Fig. 2(a1) can be calculated by $I_{up} \approx I_{down} \approx 3\mu W$, $\Delta_L = 50$ MHz and $\Delta_R = 70$ MHz. According to Eq. (5), the nonreciprocity area is

$$S = S_1 + S_2 \propto \Delta_L I_{up}/2 + \Delta_R I_{down}/2 = 180\mu W{\cdot}MHz.$$

Comparing with the frequency offset $\Delta\nu$, the impact of the intensity difference ΔI on the NB phenomenon is almost negligible. The NB phenomenon can be reflected directly by the frequency offset $\Delta\nu$, so we mainly emphasize the frequency offset under different parameters of detunings and powers. For example, when $\Delta\nu$ shrunk almost to zero, we can say that the NB phenomenon almost disappeared. Decreasing detuning Δ_1 from Fig. 2(a1)–(a4), n_2 is decreasing synchronously. According to Eq. (7), the frequency offset $\Delta\nu$ is in direct proportion to the changing of the nonlinear refractive index $\Delta n'$. Therefore, $\Delta\nu$ get its minimum value 38.6 MHz in Fig. 2(a4). With Δ_1 decreasing from top to bottom, the resonant window shifts with the speed $d\Delta_{ac}/d\Delta_1 = 2/(1 - G_4/(G_4^2 + 4|gN^{1/2}|^2)^{1/2})$ ($|d\Delta_{ac}/d\Delta_1| > 2$) where the primary and secondary splitting are caused by dressing field $\boldsymbol{E}_4$ and $gN^{1/2}$, respectively. We get the enhancement condition: $\Delta_1 + \lambda'_+ + \lambda_{1++} = 0$. The maximum intensity of the $\boldsymbol{E}_{S1}$ signal is shown in Fig. 2(a3) where $\Delta_1 = 0$ and all resonant conditions $\Delta_1 + \Delta_4 = 0$, $\Delta_1 - \Delta_2 = 0$, and $\Delta_1 - \Delta_{ac} = 0$ are satisfied. In Fig. 2(b), with $\boldsymbol{E}_2$ beam on and $\boldsymbol{E}_4$ beam blocked, we display $\boldsymbol{E}_{S2}$ signals versus Δ_{ac} at different Δ_2. The baseline represents the mixing of $\boldsymbol{E}_F$ and $\boldsymbol{E}_{S2}$ at $\Delta_1 + \Delta_2 = 0$. The peaks (shift with a speed of $d\Delta_{ac}/d\Delta_2 = G_2^2/2g^2N$) represent the enhancement cavity modes of $\boldsymbol{E}_{S2}$ by terms g^2N/d_5 and $gN^{1/2}/d_5$ in Eq. (4). The maximum value is observed in Fig. 2(b1) where $\Delta_2 = 0$ with both $\Delta_1 + \Delta_2 = 0$ and $\Delta_1 - \Delta_{ac} = 0$ satisfied. In Fig. 2(c), the frequency offset $\Delta\nu$ is caused by the different $|G_{S2}|^2/\Gamma_{00}$ on two edges in Eq. (4), respectively. By focusing on the term $|G_2|^2/d_2$ mentioned in Eq. (8) and decreasing the value of detuning Δ_2 in Fig. 2(b1)-2(b4), $\Delta\nu$ decreasing from 79.8 MHz to 60.6 MHz and n_2 reaches the maximum value in Fig. 2(b1). Comparing Fig. 2(a) and Fig. 2(b), the frequency offset is larger in Fig. 2(b) because of the stronger cavity modes of $\boldsymbol{E}_{S2}$. In Fig. 2(c), we perform this experiment by fixing $\Delta_1 = -35$ MHz and $\Delta_4 = 35$ MHz to satisfy the resonance condition $\Delta_1 + \Delta_4 = 0$ and scan Δ_{ac} at different Δ_2 with all beams on. The baseline represents the mixing cavity modes of $\boldsymbol{E}_F$ and $\boldsymbol{E}_{S1}$. The peaks in Fig. 2(c) are the cavity modes of $\boldsymbol{E}_{S2}$ with decreasing Δ_2 which get the maximum value in Fig. 2(c1) with $\Delta_1 + \Delta_4 = 0$, $\Delta_1 + \Delta_2 = 0$ and $\Delta_1 - \Delta_{ac} = 0$ are all satisfied. The

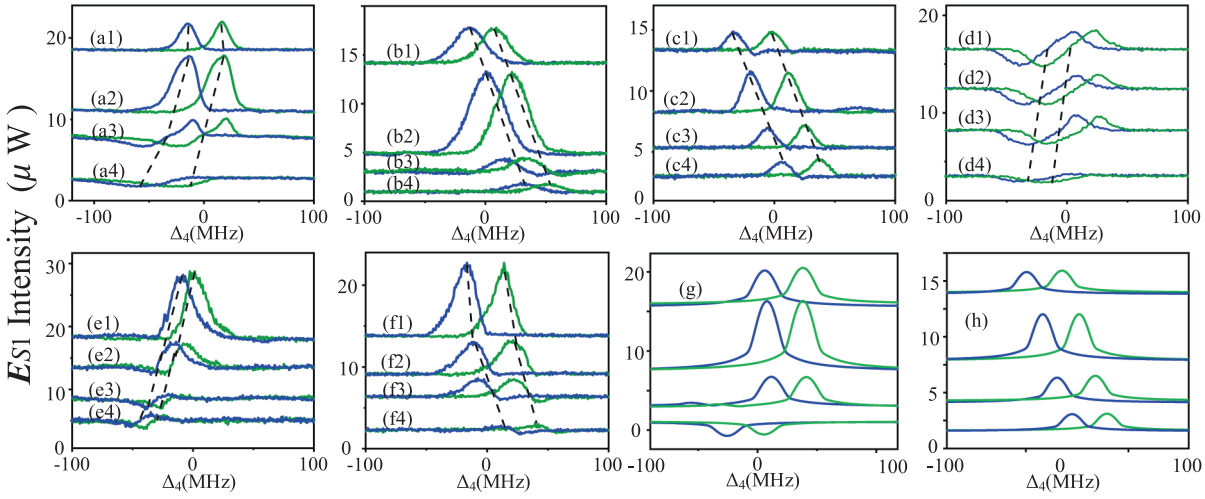

Fig. 3. Measured cavity modes of SWM versus Δ_4. (a1)–(a4) at discrete Δac as −15 MHz, 0 MHz, 15 MHz, 30 MHz, respectively, with beam $\boldsymbol{E}_2$ blocked. (b1)–(b4) at discrete Δ_1 as 0 MHz, −15 MHz, −30 MHz, −45 MHz, respectively, with beam $\boldsymbol{E}_2$ blocked. (c1)–(c4) at discrete Δ_3' as 30 MHz, 0 MHz, −30 MHz, −60 MHz, respectively, with beam $\boldsymbol{E}_2$ blocked. (d1)–(d4) at discrete Δ_4 as 30 MHz, 0 MHz, −30 MHz, −60 MHz, respectively, all beams on. (e1)–(e4) at discrete Δac as −30 MHz, 0 MHz, 30 MHz, 60 MHz, respectively, all beams on. (f1)–(f4) at discrete Δ_1 as −15 MHz, 0 MHz, 15 MHz, 30 MHz, respectively, all beams on. (g) and (h) the theoretical calculation of (a) and (c), respectively.

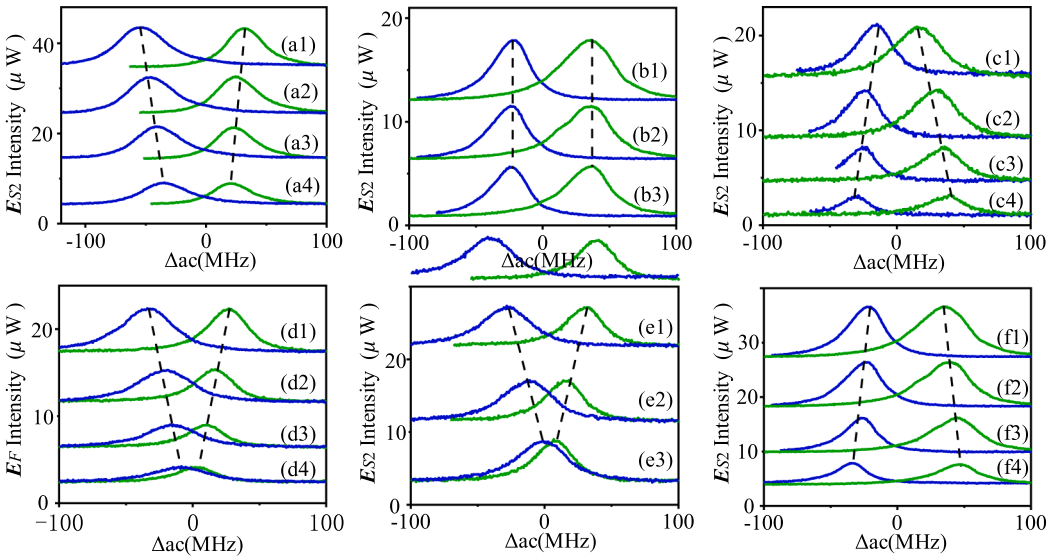

Fig. 4. Measured SWM signals intensity versus Δac. (a)–(c) with beam E4 blocked at different power of $\boldsymbol{E}_1$, $\boldsymbol{E}_2$, and $\boldsymbol{E}_3'$, respectively. (d) corresponds to (a) with beams $\boldsymbol{E}_4$ and $\boldsymbol{E}_2$ blocked. (e) and (f) are corresponding to (b) and (c) with all beams on.

feedback dressing terms $|G_{S1}|^2/\Gamma_{00}$ and $|G_{S2}|^2/\Gamma_{00}$ in Eq. (5) and Eq. (6) work together and result in the maximum frequency offset $\Delta\upsilon = 94.0$ MHz in Fig. 2(c1). With Δ_2 decreasing from top to bottom, $\Delta\upsilon$ becomes 68.1 MHz in Fig. 2(c4) with the same tendency as shown in Fig. 2(b). n_2 gets the maximum value in Fig. 2(c1) and decreasing from Fig. 2(c1) to Fig. 2(c4). When we compare Fig. 2(c) with Fig. 2(a) and 2(b), one can find that the $\Delta\upsilon$ is largest in Fig. 2 (c) with both $\boldsymbol{E}_{S1}$ and $\boldsymbol{E}_{S2}$ cavity modes enhancing the NB phenomenon.

The two different output states in Fig. 2 can be used as wavelength division multiplexing. For the division of different states, we use the channel equalization ratio, $P = 1 - [S/S_i]^2$, to measure the cleanliness of different states, where S is the area of one peak, and S_i is the area of the non-overlapping region between two different states. The minimum value of P is calculated as 75%. Besides, we use the optical contrast to divide the peak and the baseline, we use the optical contrast for the switching application, which can be defined as $C = (I_1 - I_0)/(I_1 + I_0)$, where I_1 and I_0 are the intensity at the peak and baseline positions, respectively. The value of C is calculated to be nearly 100% in Fig. 2.

Next, we investigate the NB phenomenon of dressing enhancement (or suppression) and SWM polaritons. Fig. 3(a) is the $\boldsymbol{E}_{S1}$ signals versus Δ_4 at discrete Δ_{ac} with $\boldsymbol{E}_2$ blocked. The peaks are the cavity modes of $\boldsymbol{E}_{S1}$, whose shift indicates satisfied the condition $(1)/2 < |d\Delta_4/\Delta_{ac}| < 1$ with decreasing Δ_{ac}. The baseline corresponds to the $\boldsymbol{E}_F$ cavity mode. The primary splitting is caused by external-dressing term $gN^{1/2}$ whose eigenvalue is $\lambda'_+ = [\Delta\Delta_{ac} + (\Delta_{ac}{}^2 + 4|gN^{1/2}|^2)^{1/2}]/2$ and the secondary splitting is caused by the external-dressing field $\boldsymbol{E}_4$ whose eigenvalue is $\lambda^2_{++} = [\Delta'_4 + (\Delta'_4{}^2 + 4|G_4{}^2|^2)^{1/2}]/2$. In Fig. 3(a1) and (a2), two peaks meet the enhancement conditions of $\Delta_1 + \lambda'_+ + \lambda^2_{++} = 0$. It reaches a maximum in Fig. 3(a2) at $\Delta_{ac} = 0$ MHz due to the enhancement of SWM induced by $\boldsymbol{E}_4$ where both $\Delta_1 + \Delta_4 = 0$ and $\Delta_1 - \Delta_{ac} = 0$ are satisfied. The cavity effect is relatively strong around $\Delta_{ac} = -15$ MHz, which results in the signals, as shown in Fig. 3(a1) and Fig. 3(a2) higher than the average of the baseline profile. In Fig. 3(a3), the signal is semi-suppressed and semi-enhanced because of the conditional conversion between the suppression condition ($\Delta_1 + \Delta_4' = 0$) and the enhancement condition ($\Delta_1 + \lambda_{\pm} + \lambda_{+\pm} = 0$). Fig. 3(a4) shows the purely suppressed signals in which the dips, including SWM polaritons and dressing suppression by $\boldsymbol{E}_4$. There exists a competition

between them as shown in Fig. 3(a4). In this case, the SWM polaritons become the smallest at off-resonate point ($\Delta_1 \neq \Delta_{ac}$) and the cavity dressing is satisfying the suppression condition ($\Delta_1 + \Delta_4' = 0$). In Fig. 3(a1), because of the different feedback dressing terms I_{up} and I_{down}, the frequency offset $\Delta\upsilon$ is 31.9 MHz. With the detuning Δ_{ac} decreasing from Fig. 3(a1)–(a4), the two-photon process (Δ_1–$\Delta_4 = 0$) has been modified by the nested-cascade scheme dressing (g^2N/d_5), which results in the maximum n_2 ($\Delta\upsilon = 41.6$ MHz) in Fig. 3(a4). Comparing with the results of Fig. 2 versus Δ_{ac}, we can find that there exists the NB phenomenon in the dressing enhancement (or suppression) of the SWM process. Fig. 3(g) shows the simulations corresponding to Fig. 3(a) which are in good agreement with the obtained observations. Fig. 3(b) and (c) are corresponding to Fig. 3(a) when we changed the detunings Δ_1 and Δ_3' with $\boldsymbol{E}_2$ blocked. In Fig. 3(b), peaks are the cavity modes of $\boldsymbol{E}_{S1}$. These peaks shift satisfying $d\Delta_4/d\Delta_1 = -2/(1 + gN^{1/2}/((gN^{1/2})^2 + 4|G_4|^2)^{1/2})$ with the decreasing Δ_1. The maximum intensity of the signal is shown in Fig. 3(b2) with $\Delta_1 = -15$ MHz. In Fig. 3(c2), we get the maximum value of the cavity mode of $\boldsymbol{E}_{S1}$ signal at $\Delta_3' = 0$. $\Delta\upsilon$ in Fig. 3(b1)–(b4) is changing from 21.8 MHz to 22.5 MHz. In Fig. 3(c1)–(c4), $\Delta\upsilon$ is changing from 32.9 MHz to 30.3 MHz. With the detuning Δ_1 (Δ_3') adjusted from top to bottom, n_2 gets the maximum value in Fig. 3(b1) and (c4) because of the nested-cascade scheme dressing terms $|G_4|^2/d_4$ and $|G_1|^2/\Gamma_{00}$ ($|G_3|^2/d_3$). Fig. 3(h) is the simulation corresponding to Fig. 3(c) which agrees well with the experimental results. To investigate the NB phenomenon of SWM comprehensively, we scan Δ_4 at discrete Δ_2 with all beams on. The baselines are the cavity modes of $\boldsymbol{E}_F$ in Fig. 3(d). With Δ_2 decreasing from top to bottom, the peaks (stand for the dressed cavity modes of $\boldsymbol{E}_{S1}$ by $\boldsymbol{E}_2$) are decreased. Fig. 3(e) is corresponding to Fig. 3(d) when we scan Δ_4 at discrete Δ_{ac}. The baseline is the combination of the $\boldsymbol{E}_F$ and $\boldsymbol{E}_{S2}$ cavity modes and the peaks or dips on the baseline are cavity modes of $\boldsymbol{E}_{S1}$ signals which were generated and circulate inside the cavity. With Δ_{ac} increasing, the highest enhancement peak is observed in Fig. 3(e1) with $\Delta_{ac} = -30$ MHz while Fig. 3(e2)–(e4) is semi-suppressed and semi-enhanced signals satisfying the suppression and enhancement conditions $\Delta_1 + \Delta_1' = 0$ and $\Delta_1 + \lambda_{\pm} + \lambda_{+\pm} + \lambda_{++\pm} + \lambda_{+++\pm} = 0$, respectively. In Fig. 3(d) (Fig. 3(e)), $\Delta\upsilon$ is changed from 17.8 MHz to 24.5 MHz (10.5 MHz to 12.5 MHz). In Fig. 3(f), we scan Δ_4 at discrete Δ_1 with all beams on. The baseline represents the mixing of $\boldsymbol{E}_F$ and $\boldsymbol{E}_{S2}$ cavity modes while the peaks are the cavity modes of $\boldsymbol{E}_{S1}$. To fix $\Delta_1 = -15$ MHz, we get the maximum enhancement peak in Fig. 3(f1) with $\Delta_1 + \Delta_2 = 0$ satisfied. Fig. 3(f2)–(f4) are semi-suppressed and semi-enhanced signals caused by the suppression and enhancement conditions $\Delta\Delta_1 + \Delta_2 = 0$ and $\Delta_1 + \lambda_{\pm} = 0$.

In Fig. 4, we investigate the power dependence of the NB phenomenon of SWM polaritons and enhancement (or suppression) signals

versus Δ_{ac} at $\Delta_1 = \Delta_4 = \Delta_2 = 0$. In Fig. 4(a), the peaks are the cavity modes of $\boldsymbol{E}_{S2}$ when scanning the detuning Δ_{ac} with beam $\boldsymbol{E}_4$ blocked and increasing the power of $\boldsymbol{E}_1$ (P_1). The primary enhancement condition caused by cavity is $\Delta_1 + \lambda'_+ = 0$ and the secondary enhancement condition caused by cavity feedback dressing of SWM is $\Delta_1 + \lambda'_+ + \lambda^3_{++} = 0$ ($\lambda^3_{++} = [(\Delta_s + \Delta_s^2 + 4|G_s|^2)^{1/2}]/2$). The signals in two edges of the ramp satisfy the different enhancement conditions because of the different feedback intensities of G_S. Fig. 4(d) shows the cavity modes of $\boldsymbol{E}_F$ signal with the increased P_1 from 0.6 mW (top) to 23.8 mW (bottom) with beams $\boldsymbol{E}_2$ and $\boldsymbol{E}_4$ blocked. The frequency offset $\Delta\nu$ becomes smaller (58.8 MHz to 14.5 MHz in Fig. 4(d1)–(d4)). Fig. 4(a) has one additional signal $\boldsymbol{E}_{S2}$ compared with Fig. 4(e) which induces the larger $\Delta\nu$ (85.4 MHz to 55.4 MHz in Fig. 4(a1)–(a4)) and larger intensity of MWM signals (about two times larger than Fig. 4(e)). So, one can conclude that the SWM signal enhanced the NB phenomenon. In Fig. 4(b) and (e), we investigate the cavity modes of $\boldsymbol{E}_{S2}$ against Δ_{ac} at different power of $\boldsymbol{E}_2$ (P_2) with $\boldsymbol{E}_4$ blocked or opened. In Fig. 4(b), the baselines are the cavity modes of $\boldsymbol{E}_F$. When we increase the power of P_2 from 1.1mW (top) to 19.7mW (bottom), $\Delta\nu$ is consistent as $\boldsymbol{E}_4$ is blocked. While in Fig. 4(f), with $\boldsymbol{E}_4$ opened, n_2 is decreasing with the increasing P_2 due to the term $|G_4|^2/d_4$ in Eq. (8). The decreasing nonlinear refractive index n_2 results in the decreasing frequency offset $\Delta\nu$ (from 61.7 MHz to 10.2 MHz as shown in Fig. 4(e1)–(e3)). In Fig. 4(c) and (f), we measured SWM signals versus Δ_{ac} at different power of $\boldsymbol{E}_3'$ (P_3') with $\boldsymbol{E}_4$ blocked and opened. When P_3' is decreasing from 28mW (top) to 10 mW (bottom) in Fig. 4(c), n2 is increasing due to the nested-cascade scheme dressing terms $|G_3|^2/d_3$ and $|G_4|^2/d_4$. In Fig. 4(c) and (f), we can clearly see that $\Delta\nu$ becomes larger (31.4 MHz to 70.9 MHz in Fig. 4(c1)–(c4) and 54.5 MHz to 81.9 MHz in Fig. 4(f1)–(f4)) with P_3' increasing.

In Figs. 3 and 4, the maximum value of channel equalization ratio P is calculated over 90% in Fig. 3(a), 3(c), 3(f), 4(a), 4(b), 4(c) and 4(f). The high channel equalization ratio is increasing with a larger frequency offset. Besides, the value of optical contrast C is calculated to be nearly 100% in Figs. 3 and 4.

Conclusion

In summary, the NB phenomenon of SWM caused by the cavity feedback effect was experimentally and theoretically researched and had been demonstrated. We found that the NB phenomenon can be controlled by the frequency detunings and powers of dressing beams which is performed by the degree of nonreciprocity area between two output states. Besides, the contribution of the frequency offset to the nonreciprocity area is turn out to be more obvious than the intensity difference. The detunings of incident beams can control the movements of SWM. Moreover, the channel equalization ratio is contributed from the degree of nonreciprocity area. Therefore, the two different output states of one signal from the NB phenomenon can be used as an all-optical WDMA, which can potentially contribute to all-optical devices and quantum communications.

Declaration of Competing Interest

The authors declare that they have no known competing financial interests or personal relationships that could have appeared to influence the work reported in this paper.

Acknowledgments

This work was supported by the National Key Research and Development Program of China (2017YFA0303700, 2018YFA0307500), National Natural Science Foundation of China (61975159, 61605154, 11604256, 11804267, 11904279), NSF of Shaanxi Province (2016JM6029).

Appendix A. Supplementary data

Supplementary data to this article can be found online at https://doi.org/10.1016/j.rinp.2019.102822.

References

[1] Babazadeh A, Erhard M, Wang F, Malik M, Nouroozi R, Krenn M, et al. High-dimensional single-photon quantum gates: concepts and experiments. Phys Rev Lett 2017;119:180510https://doi.org/10.1103/PhysRevLett. 119.180510.
[2] Yan WB, Fan H. Single-photon quantum router with multiple output ports. Sci Reports 2014;4:04820. https://doi.org/10.1038/srep04820.
[3] Li KK, Zhang D, Raza F, Zhang ZY, Puttapirat P, Liu Y, et al. Multi-contact switch using double-dressing regularity of probe, fluorescence, and six-wave mixing in a Rydberg atom. J Chem Phys 2018;149:074310https://doi.org/10.1063/1.5034066.
[4] Zhu Y, Gauthier DJ, Morin SE, Wu Q, Carmichael HJ, Mossberg TW. Vacuum Rabi splitting as a feature of linear-dispersion theory: analysis and experimental observations. Phys Rev Lett 1990;64:2499. https://doi.org/10.1103/PhysRevLett. 64.2499.
[5] Tanji-Suzuki H, Chen W, Landig R, Simon J, Vuletić V. Vacuum-induced transparency. Science 2011;333:1266. https://doi.org/10.1126/science.1208066.
[6] Wu H, Gea-Banacloche J, Xiao M. Observation of intracavity electromagnetically induced transparency and polariton resonances in a Doppler-broadened medium. Phys Rev Lett 2008;100:173602https://doi.org/10.1103/PhysRevLett. 100.173602.
[7] Zhang Y, Nie Z, Zheng H, Li C, Song J, Xiao M. Electromagnetically induced spatial nonlinear dispersion of four-wave mixing. Phys Rev A 2009;80:013835https://doi.org/10.1103/PhysRevA.80.013835.
[8] McCormick CF, Marino AM, Boyer V, Lett PD. Strong low-frequency quantum correlations from a four-wave-mixing amplifier. Phys Rev A 2008;78:043816https://doi.org/10.1103/PhysRevA.78.043816.
[9] Slusher RE, Hollberg LW, Yurke B, Mertz JC, Valley JF. Observation of squeezed states generated by four-wave mixing in an optical cavity. Phys Rev Lett. 1985;55:2409. https://doi.org/10.1103/PhysRevLett. 55.2409.
[10] Harada KL, Mori K, Okuma J, Hayashi N, Mitsunaga M. Parametric amplification in an electromagnetically-induced-transparency medium. Phys Rev A 2008;78:013809https://doi.org/10.1103/PhysRevA.78.013809.
[11] Zlatkovic B, Krmpot AJ, Šibalić N, Radonjic M, Jelenkovic BM. Efficient parametric non-degenarate four-wave mixing in hot potassium vapor. Laser Phys Lett 2016;13:015205https://doi.org/10.1088/1612-2011/13/1/015205.
[12] Turnbull MT, Petrov PG, Embrey CS, Marino AM, Boyer V. Role of the phase-matching condition in non-degenerate four-wave mixing in hot vapors for the generation of squeezed states of light. Phys Rev A 2013;88:033845https://doi.org/10.1103/PhysRevA.88.033845.
[13] Guo MJ, Zhou HT, Wang D, Gao JR, Zhang JX, Zhu SY. Experimental investigation of high-frequency-difference twin beams in hot cesium atoms. Phys Rev A 2014;89:033813https://doi.org/10.1103/PhysRevA.89.033813.
[14] McCormick CF, Boyer V, Arimondo E, Lett PD. Strong relative intensity squeezing by four-wave mixing in rubidium vapor. Opt Lett 2007;32:178. https://doi.org/10.1364/OL.32.000178.
[15] Glassner DS, Knize RJ. Reduced angular dependence for degenerate four-wave mixing in potassium vapor by including nitrogen buffer gas. Appl Phys Lett 1995;66:1593. https://doi.org/10.1063/1.113862.
[16] Lanzerotti MY, Schirmer RW, Gaeta Alexander L. High-reflectivity, wide-bandwidth optical phase conjugation via four-wave mixing in potassium vapor. Appl Phys Lett 1996;69:1199. https://doi.org/10.1063/1.117410.
[17] Yao X, Chen HX, Wu ZK, Wen F, Zhang D, He X, et al. Vacuum induced enhancement and suppression of six-wave mixing in a ring cavity. Laser Phys Lett 2014;11:045401https://doi.org/10.1088/1612-2011/11/4/045401.
[18] Chen HX, Zhang YQ, Yao X, Wu ZK, Zhang X, Zhang YP, Xiao M. Parametrically amplified bright-state polariton of four-and six-wave mixing in an optical ring cavity. Sci Rep 2014;4:3619.
[19] Harshawardhan W, Agarwal GS. Controlling optical bistability using electromagnetic-field-induced transparency and quantum interferences. Phys Rev A 1996;53:1812. https://doi.org/10.1103/PhysRevA.53.1812.
[20] Yuan JM, Feng WK, Li PY, Zhang X, Zhang YQ, Zheng HB, et al. Controllable vacuum Rabi splitting and optical bistability of multi-wave-mixing signal inside a ring cavity. Phys Rev A 2012;86:063820https://doi.org/10.1103/PhysRevA.86.063820.
[21] Wang H, Goorskey DJ, Xiao M. Bistability and instability of three-level atoms inside an optical cavity. Phys Rev A 2001;65:011801https://doi.org/10.1103/PhysRevA.65.011801.
[22] Zhang ZY, Cheng H, Zhang L, Zhang D, Li X, Zhang Y, Zhang YP. Unveiling the relationship between optical bistability and vacuum Rabi splitting. EPL 2017;117:53001. https://doi.org/10.1209/0295-5075/117/53001.
[23] Li KK, Bu R, Wang XX, Chen HX, Zhang D, Li XH, et al. Flip-flop converter of dual-bistability using cavity and parametric amplification four-wave mixing. Sci Reports 2018;8:2492. https://doi.org/10.1038/s41598-018-20962-5.
[24] Gauthier DJ, Malcuit MS, Gaeta AL, Boyd RW. Polarization bistability of counterpropagating laser beams. Appl Phys Lett 1990;64:1721. https://doi.org/10.1103/PhysRevLett. 64.1721.
[25] Ackemann T, Heuer A, Logvin YA, Lange W. Light-shift-induced level crossing and resonatorless optical bistability in sodium vapor. Phys Rev A 1997;56:2321. https://doi.org/10.1103/PhysRevA.56.2321.
[26] Li KK, Bu R, Zhang D, Li XH, Wen MY, Nan TH, et al. Optical bistablility in six-wave

mixing parametrical amplification. Opt Express 2017;25:023556https://doi.org/10.1364/OE.25.023556.
[27] Li KK, Tang HJ, Ahmed I, Gu BL, Wang K, Yang GG, et al. Two-channel router of phase control optical nonreciprocity in parametric amplified four-wave mixing. IEEE Photon. Tech. Lett. 2018;30:561. https://doi.org/10.1109/LPT.2018.2805020.
[28] Wang DW, Zhou HT, Guo MJ, Zhang JX, Evers J, Zhu SY. Optical diode made from a moving photonic crystal. Phys Rev Lett 2013;110:093901https://doi.org/10.1103/PhysRevLett. 110.093901.
[29] Wang Z, Chen AX, Bai YF, Yang WX, Lee RK. Coherent control of optical bistability in an open Λ-type three-level atomic system. J Opt Soc Am B 2012;29:2891. https://doi.org/10.1364/JOSAB.29.002891.
[30] Zhu ZH, Chen AX, Yang WX, Lee RK. Phase knob for switching steady-state behaviors from bistability to multistability via spontaneously generated coherence. J Opt Soc Am B 2014;31:2061. https://doi.org/10.1364/JOSAB.31.002061.
[31] Zhang ZY, Ma DM, Liu J, Sun YY, Cheng L, Khan GA, et al. Comparison between optical bistabilities versus power and frequency in a composite cavity-atom system. Opt Express 2017;25:8916. https://doi.org/10.1364/OE.25.008916.
[32] Du YG, Zhang YP, Zuo CC, Li CB, Nie ZQ, Zheng HB, et al. Controlling four-wave mixing and six-wave mixing in a multi-Zeeman-sublevel atomic system with electromagnetically induced transparency. Phys Rev A 2009;79:063839https://doi.org/10.1103/PhysRevA.79.063839.
[33] Li CB, Zhang YP, Nie ZQ, Du YG, Wang RM, Song JP. M, Xiao, Controlling enhancement and suppression of four-wave mixing via polarized light. Phys Rev A 2010;81:033801https://doi.org/10.1103/PhysRevA.81.033801.
[34] Zhang Y, Khadka U, Anderson B, Xiao M. Temporal and spatial interference between four-wave mixing and six-wave mixing channels. Phys. Rev. Lett. 2009;102. https://doi.org/10.1103/PhysRevLett. 102.013601.